

A Practical BLDC Motor Design Procedure for Diver Propulsion Vehicle Applications

Yannis L. Karnavas, *Member, IEEE*, Ioannis D. Chasiotis, *Student Member, IEEE* and D. N. Stravourellis

Abstract -- In this paper a practical approach for the design and construction of a brushless DC motor (BLDCM) for a diver propulsion vehicle (DPV) is presented. After evaluating the corresponding vehicle's characteristics, a three step process is proposed and followed. For economical reasons and rapid prototyping, an appropriate motor stator found in the market is utilized. Thus, the required B-H curve of the material is extracted experimentally in the first step, whose knowledge is necessary for the motor design phase. Secondly, considering the DPV's thrust requirements, a suitable propeller is studied, designed and selected which in turn leads to the BLDCM requirements for torque and speed. Having the stator geometry known, the outer rotor BLDCM theory is followed in the third step where, with the help of a custom developed software code, the remaining variables are calculated pertaining to the windings, rotor and permanent magnet parts. Finally, relevant results are shown by studying the motor topology using FEM.

Index Terms-- Brushless DC motor, outer rotor, permanent magnet motor design, diver propulsion vehicle (DPV)

I. INTRODUCTION

Over the years, technological advances in the scuba industry have improved the sport tremendously. More compressed air became available through the use of larger capacity tanks, better regulators were designed to make it easier to breath at depth and computers improved dive-time management. These advances made diving more accessible to the average diver, as well as making it a more technical sport. The average diver's excursion under water used to be limited to exploring relatively small areas close to the point of entry, however, the sophisticated regulators and computers opened new horizons for the serious and not so serious divers alike [1,2]. Coupled with the technological advances in scuba came a growing interest in underwater transportation, which has brought several companies into a rapidly expanding market that once was reserved for only military and commercial divers.

There are primarily two types of underwater transportation systems for recreational and technical divers; the diver propulsion vehicle (DPV) and the underwater scooter. Usually (but not always) the difference between a DPV and a scooter is that a DPV is a vehicle that one can physically ride with an integrated saddle while a scooter is a unit that tows the diver along by the arms. A more general rule is that scooters tend to have smaller capacity battery than the DPV. Apart from recreational activities, there are more and more jobs that require long-lasting submarine stays and are done

by automatic systems or divers. Tasks such as submarine welding, submarine installation and maintenance, status control and dock maintenance, and the operation and maintenance of fish farms involve tasks requiring low power electric propulsion applications. The advantages of using such applications are to make better use of the diver's available time, based on the capacity of the oxygen reservoirs, respectively the use of smaller tanks for the same residence time, as their travel time is reduced underwater. It also achieves a quicker approach to points of interest when required (breakdowns, failures or accidents).

Although technical literature on autonomous underwater vehicles (AUV) as well as remotely operated vehicles (ROV) has been grown to a large extend over the years e.g. [3-5], the corresponding one dedicated to DPVs is not so extensive. Most of the research is towards the hydrodynamic features, sensors, mapping, and the control strategies from a robotic perspective [6,7]. So, the electrical motor part seems not to have gained the necessary attention and has not yet been sufficiently addressed [8]. In this context, the authors believe that this effort could provide some useful information especially from a practical point of view.

The paper is organized as follows: DPV information and requirements are first set in Section II. The DPV required propeller is designed in Section III based on typical thrust settings found in commercial DPV counterparts. In Section IV, an appropriate stator available on the market is utilized whereas its magnetizing curve is experimentally extracted. Section V describes the BLDCM design process along with relevant results obtained from FEM analysis and also a prototype construction is presented. Finally, Section VI concludes the work.

II. DIVER PROPULSION VEHICLES CHARACTERISTICS AND PROBLEM STATEMENT

A DPV construction is significantly smaller than their larger counterparts i.e. AUV and much more cost-effective since the price of the most expensive ones can reach 13,000€. A DPV's external view can be seen in Fig. 1. It consists of the hull and the propeller along with its protector externally, while the batteries, the motor and some control circuits are



Fig. 1. A typical commercial DPV in the 300W motor power range.

Y. L. Karnavas, I. D. Chasiotis and D. N. Stravourellis are with the Electrical Machines Laboratory, Department of Electrical and Computer Engineering, Democritus University of Thrace, Xanthi, GR-67100, Hellas (e-mail: karnavas@ee.duth.gr, ichasiot@ee.duth.gr, dimistra@ee.duth.gr).

Brand/ Model	Battery Voltage/ Capacity (V/Ah)	Speed (km/h)	Run Time (min)	Current Range (A)	Input Power (W)	Overall Length (m)
<i>Oceanic Mako</i>	12/17	2.4-4.3	40-120	8.5-11.3	100-135	0.635
<i>Torpedo 2000</i>	12/32	3.6	50-80	42-42	504	0.914
<i>Farallon MK8</i>	24/18	4.75	60-115	10-18	240-432	1.574
<i>AUL Drako</i>	24/36	6.0	120+	18-18	432	1.828
<i>Predator 2000</i>	24/18	4.5	40-100	12-30	288-720	1.168

located inside, giving more choice and comfort to more expensive versions. For the purposes of this study, Table I presents typical DPVs characteristics currently retrieved from commercial manufacturers' datasheets. Generally, they are powered by two to four 12V batteries and depending upon the configuration the latter are wired in series or in series-parallel. Smaller DPVs average 0.6 meters in length, and the larger ones can be up to three times longer. Range capability varies by model but will generally run from one to five miles, depending also on the current drawn by the motor which is in the range of 8 up to even 30 A with corresponding power of 100 W up to approximately 700 W. A crucial quantity is the travelling speed which as can be seen from the Table is varying from 2.5-6 km/h. Thus, the problem here refers to a combined propeller-motor system design investigation so as to meet requirements based on the above.

III. PROPELLER DESIGN

OpenProp is an open source software (implemented in Matlab code) primarily developed in MIT, that can be used to design, analyze, and build optimized propellers and horizontal axis turbines [9]. The numerical model is based on the Propeller Lifting Line Theory, which is used in parametric software packages by the US Navy and commercial designers. In parametric mode, *OpenProp* enables the user, after identifying the propeller's requirements, to arrive at the selection of its attributes by comparing performance to all combinations of blade number, propeller diameter, and rotational speed [10]. Thus, the user enters the above quantities and the program calculates all possible propeller solutions that meet the input values and lists performance/ diameter/ speed/ rotation curves so as to make clear which combination presents the best performance.

A. Parametric Study

The parametric investigation conducted here considered the following: a) number of blades; 3-6 in step of 1, b) rotational speed; 700-1400 rpm in step of 100, c) propeller diameter; 100-400mm in step of 10. The speed range of the propeller was selected from the data found by the commercial DPVs while the propeller diameter -after an initial investigation- was selected in the range where the propeller could produce the output thrust requirements and at the same time was not much larger than the estimated diameter of all

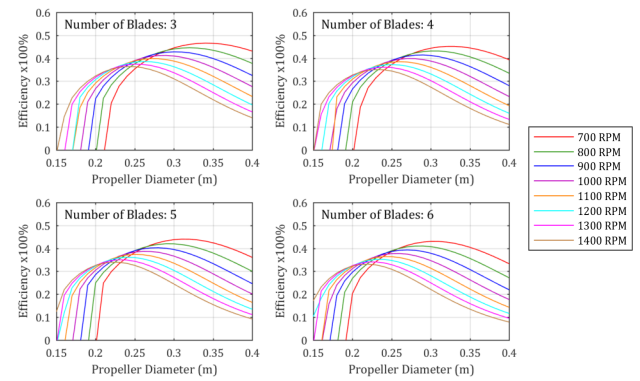


Fig. 2. Propeller efficiency results obtained from DPV parametric analysis.

the DPVs. Figure 2 shows the parametric results obtained. Analyzing these results we can draw the following conclusions: a) after a certain diameter value, the increasing number of blades along with the increasing speed leads to less efficient designs; this, combined with an economic solution leads to a 3 blade propeller selection, b) in all cases, a diameter increment above 0.24 m approximately, causes small variations in performance throughout the examined speed range and c) for a diameter value close to 0.3 m the efficiency variation versus speed is quite small; therefore the diameter of 0.29 m was chosen.

B. Single Propeller Design

Having limited the possible topology and propeller characteristics solutions by investigating the performance through a large number of combinations, we ended up with a propeller that could work more efficiently at the required thrust. Next, in *OpenProp*'s single propeller design mode, the program input data are very specific and based on these, the final propeller topology is then derived. The user defines now: a) the number of blades, b) the rotational speed, c) the propeller diameter, d) the required thrust, e) the vehicle's speed and f) the propeller hub diameter. Table II shows the final propeller calculated characteristics along with the estimated power needed by the driving motor. By post-processing of the software output the user can fully implement the propeller in a CAD software e.g. Solidworks as can be seen in Fig. 3.

Diameter (tip-to-tip)	0.29 m	Thrust	200 N
Rotational speed	990 rpm	Power	404.3 W
DPV Speed	1 m/s	Torque	3.9 Nm

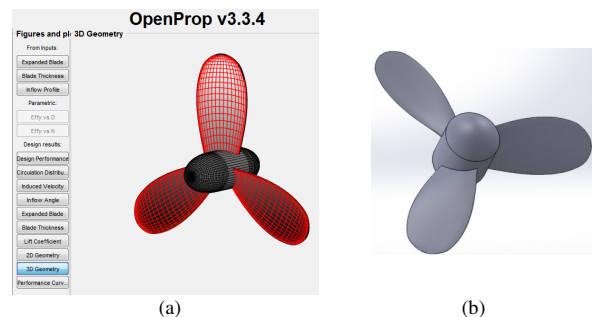


Fig. 3. Final propeller visualization result a) OpenProp view, b) Solidworks 3D model using OpenProp results.

IV. BLDC STATOR CONSIDERATIONS

For this study, a motorcycle stator was utilized as a fair solution. These stators can be found easily at low cost and in many forms and dimensions. With this option, the design of the motor is greatly simplified and the prototyping becomes easier. Diameters, teeth, slots dimensions and axial length are known and considered fixed, thus the design actually focus on the rest of the parameters. However, a necessary procedure in this case, is the experimental evaluation of the stator's ferromagnetic material magnetization characteristic (B-H curve) in order to be known at the next stage of the motor design. For cases of toroidal specimens such as our stator core, the apparatus shown in Fig. 4(a) may be used to perform the appropriate measurements [11]. Fig. 4(b) shows the corresponding experimental setup used. Let the primary winding to be denoted as "main" having N_{main} turns and the secondary as "sense" having N_{sense} turns. Then, the time dependent magnetic field intensity H as a function of the geometry of the toroid and the ampere-turns of the main winding can be described by,

$$H(t) = \frac{N_{main} i_{main}}{l_{core}} \quad (1)$$

Here the l_{core} is the length of the mean path of the flux lines in the core and is equal to the mean perimeter within the toroidal part (R_{si} , R_{sb} with respect to Fig. 5.b),

$$l_{core} = \pi(R_{si} + R_{sb}) \quad (2)$$

In order for a typical iron core to become deeply saturated, the magnetic field intensity needs to be in the range of 8 kA/m up to 16 kA/m. With the point of interest being the area where we have the greatest changes in the slope of the curve (i.e. knee) and since this area is encountered before deep saturation, a peak magnetic field strength $H_{peak}=12$ kA/m was chosen. This option mitigates the requirement for very large currents in the windings of the core or, respectively, the requirement for a large number of turns to achieve the desired magnetic field strength H . Thus, in our experiment Eq. (1) gives $N_{main} \cdot i_{main} = 2559.77$ A-turns. ($l_{core}=0.2133$, R_{si} and R_{sb} are given in Table III). By selecting 160 turns for N_{main} (to obtain 9 turns per slot between the stator teeth), a current of 16 A must be supplied to reach the desired magnetic field strength H in the core (12000 A/m). A wire cross section of 1.29 mm (AWG 16) is more than enough for this current, offering also a margin of safety. This cross section has a resistance 13 Ω /km leading the length of the main winding to be 9.7 m with a corresponding total resistance 0.126 Ω . Thus, the required supply voltage of the primary winding can be easily found to be 2.015 Volts. The magnetic flux density can be calculated by sampling the V_{sense} voltage in the sensing winding by the following formula:

$$B(t) = \frac{\lambda(t)}{A_{core} N_{sense}} \quad (3)$$

where A_{core} is the cross section of the core and $\lambda(t) = \int V_{sense} dt$ which for a sampling process with sampling interval Δt can be calculated by

$$\lambda_{k+1} = \lambda_k + V_{sense,k} \Delta t \quad (4)$$

The required number of measurements k is proposed to be between 400-2000 for every two periods. Since the supply

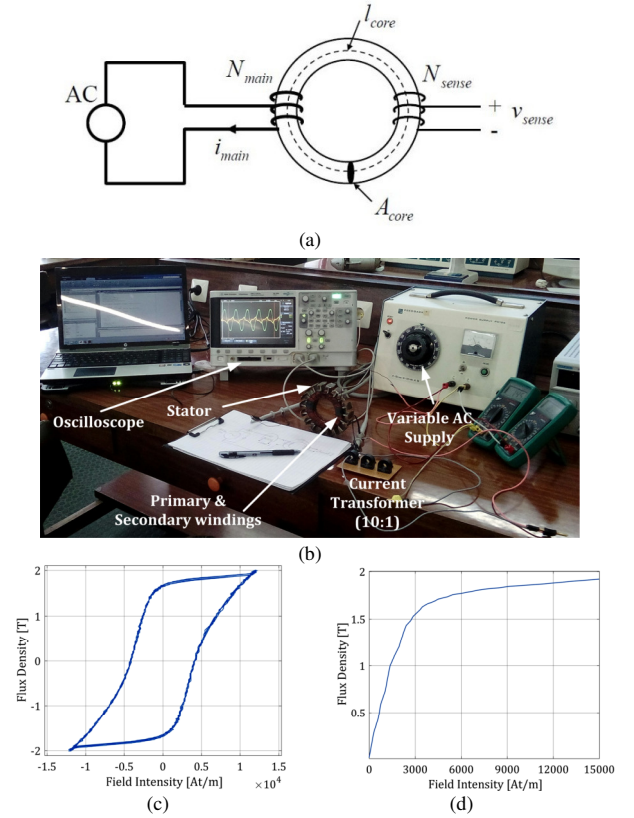


Fig. 4. B-H experiment: a) theoretical circuit, b) laboratory setup, c) B-H loop from processed samples and d) material B-H curve used for the design.

voltage period is 20ms, the minimum sampling frequency should be $f_s = 10$ kHz ($T_s = 0.1$ ms for 200 samples/period) and the maximum may be $f_s = 50$ kHz ($T_s = 20$ μ s for 1000 samples/period). In this study, the maximum sampling frequency was chosen for more accurate results. It should be noted here that for proper results evaluation, the V_{sense} should not be sampled in RMS values and also, the dc component must be eliminated. This can be easily implemented in a post-processing phase by subtracting from each measurement the average value of the total measurements. Further, core losses can be calculated using the formula:

$$P_{core} = \frac{N_{main}}{N_{sense}} \frac{1}{K} \sum_{k=1}^K (V_{sense,k} \cdot i_{main,k}) \quad (5)$$

The stator core hysteresis loop resulted from the processing of the measured values is shown in Fig. 4(c). The processing of the corresponding results led to the B-H curve which is shown in Fig. 4(d) and used later (Section V) in the final motor design phase. Moreover, a comparison was made with several available curves retrieved from material databases in order to identify the steel category to which our stator may belong to. A Matlab code was written where the shape-preserving piecewise cubic interpolation was implemented using the B-H values measured from the experiment for our own material. Among the materials examined, 27 presented a relatively small error belonged to the Low Carbon Steels and Silicon Steels categories. From these comparisons (not shown here), the one with the smallest error (3.96%) refer to low carbon forge annealed alloy.

V. OVERALL BLDC MOTOR DESIGN

A. Topology and Design Parameters Considerations

Knowing the motor requirements from the propeller analysis and the stator's magnetic characteristic, the rest of the design can be examined next. To investigate any possible cases, the effect of each quantity on the motor characteristics and the choice of the final characteristics and sizes, a custom code was developed in the MATLAB environment.

Concerning the stator dimensions, many measurements were performed using mechanical and electronic caliper of a 0.05 mm precision. The final value of each dimension was averaged on the total measurements with both instruments. With respect to Fig. 5, the data obtained are given in Table III. Also, for further hydrodynamic simulations as well as for prototyping purposes, a complete model of the stator was designed in Solidworks software. From there, the area covered by the slot is calculated as $A_s=193.66 \text{ mm}^2$, while the corresponding stacking factor obtained was $k_{st}=0.8443$.

From this point on, the most important features refer to a) stator winding topology, b) the airgap, c) the rotor poles and d) the magnet type and dimensions [12]. Concentrated over distributed windings were preferred because they present lower cogging torque and offer easier construction options [13]. Also, among several winding sequences examined in Ansys Mawxell software regarding the best efficiency of the motor, the "AaAaBbBbCcCaABbBbCcC" sequence was chosen (stator has 18 slots) which is actually a modified dLRK topology found in many commercial BLDC motors [14].

Surface mounted magnets were chosen since they can be easily found in the market and also impose a straightforward prototyping. Based on this, the rotor pole number can be found if the following relationships are considered [15],

$$w_{bi} = \frac{\phi_g}{N_{sm} B_{max} k_{st} L} \quad (6)$$

$$w_{tb} = w_{bi} (2/N_{sm}) \quad (7)$$

where ϕ_g is the airgap flux, B_{max} the maximum allowed flux density in the stator and N_{sm} the number of slots per magnet. If N_{spp} is the number of slots per pole per phase and N_{ph} is the number of phases, then the number of magnets is $N_m = N_{spp} N_{ph} = N_s / N_m$. By considering typical BLDC flux value in the airgap at $\phi_g = 0.95 \text{ Wb/m}^2$ [16] and the magnetic field from the B-H curve before saturation (knee) of the material set to $B_{max} = 1.6 \text{ T}$, the number of magnets according to the geometric characteristics of the stator can then be derived as:

$$N_m = \frac{N_s w_{tb} B_{max} k_{st} L}{\phi_g} \quad (8)$$

Also, for a magnet height set to $l_m = 2.5 \text{ mm}$ (this choice will be justified next) and examining airgap lengths varying from $g = 0.5\text{--}3 \text{ mm}$, a mean value of 16.36 magnets is obtained. It is therefore chosen that $N_m = 16$ (8 pole pairs) with this option justified further because it is one of the two best choices with respect to the winding factor, which for 18 stator slots is $k_w = 0.945$ [17].

Magnet dimensions have to be determined next. Given the radial magnetization of the magnets, the maximum airgap

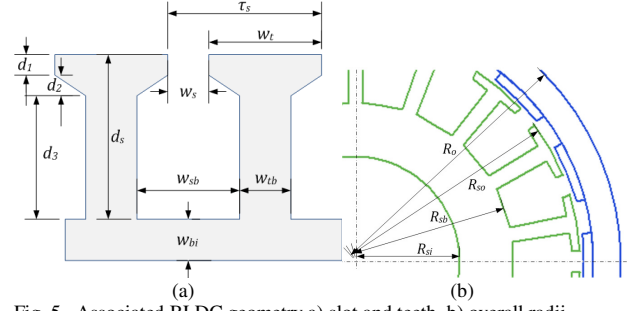


Fig. 5. Associated BLDC geometry a) slot and teeth, b) overall radii.

TABLE III
GEOMETRICAL PARAMETERS OF THE UTILIZED STATOR

Parameter	Value (mm)
Teeth leg width	w_{tb} 3.7015
Teeth shoe width	w_t 14.144
Teeth shoe height	d_1 2.054
Teeth shoe sloping height	d_2 0.7
Conductor slot depth	d_3 14.337
Stator back iron width	w_{bi} 14.236
Slot width	w_{sb} 11.411
Slot opening width	w_s 5.419
Inner slot sloping width	w_{si} 14.321
Active motor axial length	L 16.167
Total teeth height	d_s 17.091
Rotor outer radius	R_{ro} 130
Stator inner radius	R_{si} 26.9
Stator outer radius	R_{so} 57.5
Stator back iron radius	R_{sb} 41

flux density can be calculated by Eq. (9) where B_r is the flux density produced by the magnets, μ_r is the relative magnetic permeability and k_{leak} is the leakage flux coefficient.

$$B_m = \frac{B_r k_{leak}}{1 + (\mu_r g_c / l_m)} \quad (9)$$

The latter can be determined through FEM analyses but here the empirical formula shown in [18] was used,

$$k_{leak} = 100 - \left(\frac{7N_m}{60} - 3 \right) / 100 \quad (10)$$

which gave $k_{leak} = 1.011333$ for 16 rotor poles. The next variable of Eq. (9), g_c , can be specified as follows:

$$g_c = g k_{carter} \quad (11)$$

where k_{carter} is the coefficient as described in [15] which is used to take into account the different permeability in each airgap point, i.e. to determine an equivalent airgap in which the calculations due to variable permeability would not be altered. The most precise expression which considers the magnetic field curvature near the teeth is:

$$k_{carter} = \left[1 - \frac{w_s}{\tau_s} + \frac{4g}{\pi \tau_s} \ln \left(1 + \frac{\pi w_s}{4g} \right) \right]^{-1} \quad (12)$$

which in our case gives the value of 1.00057325 for an airgap of 1 mm. That means that we can consider an active gap $g = 1 \text{ mm}$ with a 0.057% error only. Having determined the above and knowing that for N35 grade neodymium magnets B_r is near 1.2 T, a parametric investigation was performed using Eq. (9) for different magnet thicknesses and their effect on B_m . Fig. 6 shows the dependence of B_m as a function of

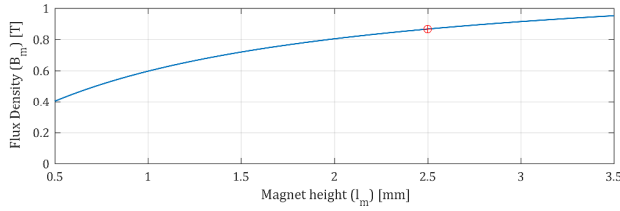


Fig. 6. Flux density as a function magnet height for $g=1$ mm and $N_m=16$.

magnet thickness (height l_m) for an airgap of $g=1$ mm and $N_m=16$. The typical standard magnet thicknesses found in the market start at 1 mm and reach up to 10 mm by a step of 0.5 mm. In order to have as much magnet material as possible leading to a lower stator current to produce the desired torque the thickness of the magnets is chosen $l_m=2.5$ mm, while the corresponding flux density for this thickness is 0.867 T.

However, the above choice has to be combined and justified by taking into account the pole-arc to pole-pitch ratio or –differently– the “embrace” of the magnet. Finding the flux density in the airgap for our given choices, we can calculate the desired flux density generated by the magnet, in the airgap, as a function of half the magnitude of the magnet, as will be explained below:

$$\vec{B}_g = \frac{4}{\pi} B_m \sin a \quad (13)$$

We focused on the fact that the values of the magnetic flux density produced by the magnet in the airgap, B_g , belongs to the interval [0.85-0.95 T] as stated in [19], thus we should investigate those values such as they were “compatible” in terms of magnet width which can be easily found in the market. Also, the variable a in Eq. (13) represents the angle occupied by half of the rotor pole - half magnet - in electric degrees. The relation that links the above variable to the magnet width is as follows,

$$w_m = \frac{2a(D-2g)}{p} \quad (14)$$

where w_m is the magnet width, p are the pole pairs and D the stator outer diameter. Substituting (13) to (14) and by considering B_g to belong to the aforementioned interval, a magnet interval of $w_m \in [14.9, 18.1]$ mm is derived. From Eq. (15) using this interval we obtain that $embrace \in [0.622, 0.7551]$.

$$embrace = \frac{w_m N_m}{2\pi(R_{st} + g + l_m)} \quad (15)$$

The aforementioned thought is depicted graphically in Fig. 7 where a parametric investigation, using the above equations, was conducted. In Fig. 7(a), the variation of B_g as a function of embrace is shown. If we consider a conservative case scenario for B_g (close to 0.85 T), i.e. equal to 0.852 T, then an embrace of 66.7% occurs. Continuing in Fig. 7(b), for an embrace of 0.667, a magnet width of 15.97 mm occurs. The commercially available magnets found close to this width and finally used, were $w_m=16$ mm.

B. FEM Analysis Evaluation and Prototype Construction

By utilizing all the data derived in the previous paragraphs, a two dimensional model was designed in a commercial finite element analysis software and the corres-

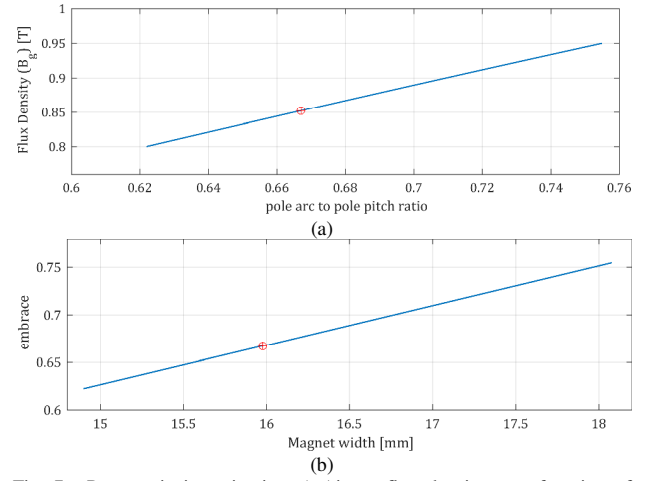


Fig. 7. Parametric investigation a) Airgap flux density as a function of magnet embrace, b) embrace as a function of magnet width.

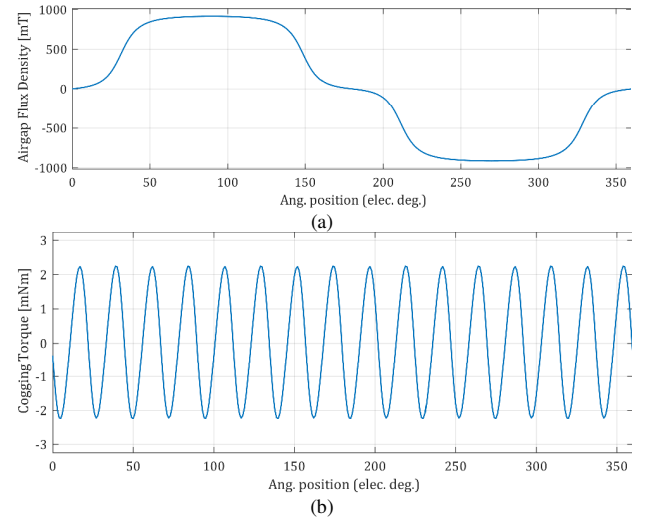


Fig. 8. FEA results from the designed BLDC motor, a) airgap flux density, b) cogging torque variation.

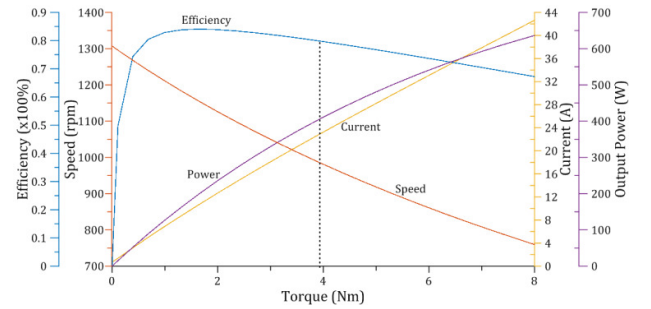


Fig. 9. Characteristic curves (efficiency, speed, current and output power as a function of torque) of the designed BLDC motor.

ponding FEM analysis was performed in order to validate our analytical design approach. The most important results from this analysis are shown here. In Fig. 8(a), the airgap flux density is depicted. From this figure it can be seen that the shape and the magnitude are satisfactory enough. Also, in Fig. 8(b) a cogging torque of 2.2 mNm is shown which is 0.057% of the rated torque (3.85Nm) and it can be considered acceptable. Also from the post-processing of the

TABLE IV
NOMINAL DATA AND PARAMETERS THE DESIGNED BLDC MOTOR

Quantity	Value	Unit
Output Power	0.4	kW
Nominal voltage	22.2	Volts
Nominal current	22.48	A
Stall current	293.6	A
Nominal torque	3.85	Nm
Stall torque	33.95	Nm
Nominal speed	990.22	rpm
Phase resistance	0.04	Ω @ 75°C
Phase inductance	3.94	μ H
Torque constant	17.55×10^{-2}	Nm/A
Back-EMF constant	15.55×10^{-2}	V/(rad/s)
Rotor inertia	5.09×10^{-3}	kg.m ²
Efficiency	80.03	%
Magnet pole embrace	66.70	%
Copper weight	0.333	kg
Stator weight	0.513	kg
Rotor weight	0.401	kg
Magnets/pole pairs	NdFeB35/8	-

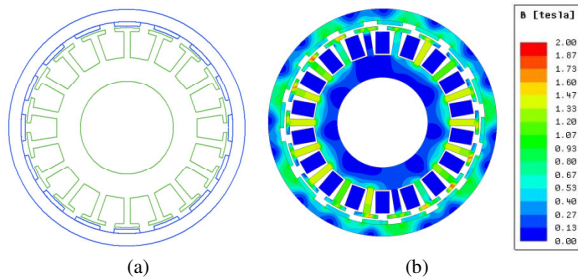


Fig. 10. Designed BLDC motor a) overall geometry and b) magnetic flux density distribution at rated operation.

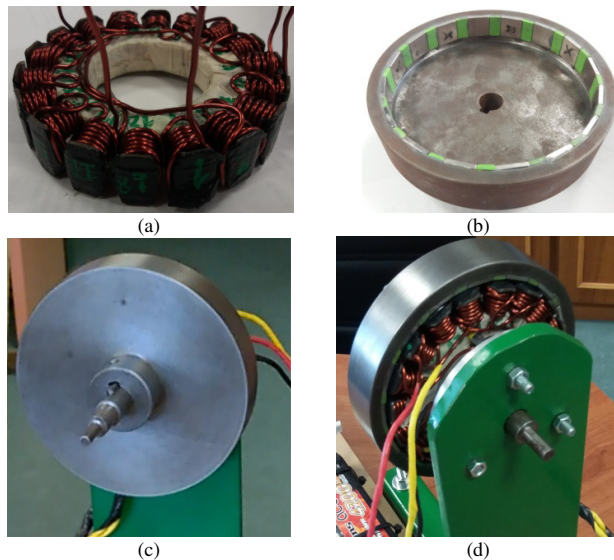


Fig. 11. Constructed BLDC motor prototype, a) completed stator with three phase windings, b) rotor with magnets in place along with 3D printed spacers (green), c) front view of assembled motor including shaft, d) rear view of the assembled motor mounted in a painted aluminum base.

FEM results, a characteristic curve chart of the motor is drawn and as it can be seen in Fig. 9, where the dotted line denotes the nominal operating point. From this chart it can be seen that the relevant requirements concerning the corresponding quantities are met. The associated motor geometry and the corresponding flux density distribution are depicted in Fig. 10. Finally, the motor main data (along with

some more parameters derived from FEA) are summarized in Table IV. For future testing, a prototype was constructed which can be seen in Fig. 11. Besides the ready-made stator and the magnets which were ordered from the market, the rotor and its shaft were machined in a CNC lathe. Stator coils were wound manually. For precise gluing of the magnets ensuring the required embrace, 3D printed spacers were used. The shaft includes appropriate diameter variations (from center to the ends), so as to ensure mechanical rigidity and also to cope for propeller and encoder mounting.

VI. CONCLUSIONS

A practical procedure for the design of an outer rotor brushless dc motor towards a diver propulsion vehicle application was presented in this paper. Without loss of generality, an appropriate stator easily found in the market is employed for keeping manufacturing cost low. Its material magnetic characteristics can be easily extracted experimentally. Also, a suitable propeller design considered as another necessary step in order for the motor requirements to be reached. Classical permanent magnet motor design theory was employed according to the specific application. FEM analysis results of the final design revealed satisfactory performance, meeting the relevant requirements and confirmed the validity of the proposed approach. A prototype has been constructed towards future work in extended testing in real environment conditions.

VII. REFERENCES

- [1] S. Kimura, G. Cox, J. Carroll, S. Pengilly, A. Harmer, "Going the distance: Use of Diver Propulsion Units, underwater acoustic navigation, and three-way wireless communication to survey Kelp Forest habitats". In: *Steller D., Lobel L., eds. Diving for Science 2012. Proceedings of the American Academy of Underwater Sciences 31st Symposium*. Dauphin Island, AL, 2012.
- [2] A.F. Molland, "The Maritime Engineering Reference Book: A Guide to Ship Design, Construction and Operation", 1st ed., Butterworth-Heinemann, Oxford, UK, 2011.
- [3] F. Song, P.E. An, A. Folleco, "Modeling and simulation of autonomous underwater vehicles: design and implementation", *IEEE Journal of Oceanic Engineering*, vol. 28, no. 2, pp. 283-296, 2003.
- [4] A. Vasiljević, Đ. Nad, F. Mandić, N. Mišković, Z. Vukić, "Coordinated navigation of surface and underwater marine robotic vehicles for Ocean sampling and environmental monitoring", *IEEE/ASME Transactions on Mechatronics*, vol. 22, no. 3, pp. 1174-1184, 2017.
- [5] K. Poore, C. Kitts, G. Wheat, W. Kirkwood, "A small scale ROV for shallow-water science operations", in *Proc. of IEEE OCEANS*, 19-23 Sep. 2016, Monterey, CA, USA, pp. 1-6.
- [6] G.T. Reader, I.J. Potter, E. Clavelle, "Power and oxygen sources for a diver propulsion vehicle", in *Proc. of IEEE OCEANS*, 5-8 Nov., 2001, vol. 2, Honolulu, Hawaii, USA, pp. 880-887.
- [7] R. Sriwijaya, J. Naibaho, Y.P. Widatama, "Design of single passenger underwater vehicle", in *Proc. of IEEE 7th Intl. Annual Engineering Seminar (InAES)*, 1-2 Aug., 2017, Yogyakarta, Indonesia, pp. 1-4.
- [8] J. Qiu, C. Shi, M. Jin, R. Lin, "Counter-rotating permanent magnet brushless DC motor for underwater propulsion", in *Proc. of the 5th Power Electronics and Motion Control Conference (IPEMC)*, vol. 2, 14-16 Aug., Shanghai, China, 2006, pp. 1-5.
- [9] B.P. Epps, J.S. Chalfant, R.W. Kimball, A.H. Techet, K. Flood, C. Chrysostomidis, "OpenProp: An open-source parametric design and analysis tool for propellers", in *Proc. of Grand Challenges in Modeling and Simulation (GCMS)*, July 13-16, 2009, Istanbul, Turkey.
- [10] E.K. Skaland, "The influence of the choice of propeller design tool on propeller performance", M.Sc. Thesis, Dept. of Marine Technology,

Norwegian University of Science and Technology (NTNU), June 2016.

- [11] IEEE Standard 393-1991, "*IEEE Standard for Test Procedures for Magnetic Cores IEEE Standard for Test Procedures for Magnetic Cores*", IEEE Power Electronics Society, 1992 (reaffirmed at 2007).
- [12] J.R. Hendershot, T.J.E. Miller, "*Design of Brushless Permanent-Magnet Machines*", 2nd. ed., Motor Design Books LLC, 2010.
- [13] G. Bara, "Comparative study of concentrated and distributed winding using Flux", CEDRAT news, N° 69, March 2016.
- [14] H.K.S. Ransara, U.K. Madawala, "A torque ripple compensation technique for a low-cost brushless DC motor drive", *IEEE Transactions on Industrial Electronics*, vol. 62, no. 10, pp. 6171-6182, Oct. 2015.
- [15] D.C. Hanselman, "*Brushless Permanent-Magnet Motor Design*", McGraw-Hill, University of Maine-Orono, 1994.
- [16] J.F. Gieras, "*Permanent Magnet Motor Technology Design and Applications*", 3rd ed., Taylor & Francis Group, New York, 2010.
- [17] S.E. Skaar, Ø.Krøvel, R.Nilssen, "Distribution, coil-span and winding factors for PM machines with concentrated windings", in *Proc. of 17th Intl. Conference on Electrical Machines (ICEM)*, Sep. 2-5, 2006, Chania, Greece, pp. 1-5.
- [18] P.M. Dusane, "Simulation of a Brushless DC motor, in ANSYS-Maxwell 3D", M.Sc. Thesis at Czech Technical University in Prague, Faculty of Electrical Engineering Department of Power Engineering, Prague, April 2016.
- [19] J. Cros, M.T. Kakhki, G.C.R. Sincero, C. Martins, P. Viarouge, "Design Methodology for Small Brush and Brushless DC Motors", In "Vehicle Engineering", Book Chapter, Academy Publish Team, eds., Dec. 2014.

VIII. BIOGRAPHIES

Yannis L. Karnavas (M'98) was born in Volos, Hellas, 1969. He received the Diploma Degree and his Ph.D. from the Department of Electrical & Computer Engineering (DECE), Democritus University of Thrace (DUTH), Xanthi, Hellas in 2002. He is with the Electrical Machines Laboratory of the DECE, DUTH as an Assistant Professor. His research interests include electrical machines design, analysis, modeling and optimization, controller design and application to electrical machines and artificial intelligence methods application to them. He has published several papers in various international journals and conferences, as well as book chapters in international engineering books. He has participated in many research projects as research leader or scientific associate. He serves as an Associate Editor and as an Editorial board member in various international scientific journals. He is a chartered electrical engineer as well as a member of Hellenic Technical Chamber. Prof. Karnavas is also an IEEE, IEEE PES, IEEE IAS and IEEE IES member.

Ioannis D. Chasiotis (SM'11) was born in Athens, Hellas, 1991. He received the Diploma Degree in electrical and computer engineering from the Department of Electrical and Computer Engineering, Democritus University of Thrace, Xanthi, Hellas. He is with the Electrical Machines Laboratory of the same Dept. where he is currently pursuing his Ph.D. degree. His research interests are in the area of electrical machines design and the development of relevant optimization methods and applications. He is student member of IEEE.

Demetrios D. Stravoullis was born in Mitilini, Hellas, 1993. He received the Diploma Degree in electrical and computer engineering from the Department of Electrical and Computer Engineering, Democritus University of Thrace, Xanthi, Hellas. He is with the Electrical Machines Laboratory of the same Department. His research interests are in the area of electrical machines design for marine electric propulsion applications.